International Journal of Nanomedicine

Dovepress
open access to scientific and medical research

Open Access Full Text Article

ORIGINAL RESEARCH

Delivery of miR-375 and doxorubicin hydrochloride by lipid-coated hollow mesoporous silica nanoparticles to overcome multiple drug resistance in hepatocellular carcinoma

This article was published in the following Dove Press journal:
International Journal of Nanomedicine
24 July 2017
Number of times this article has been viewed

Huiying Xue[1]
Zhaoyang Yu[1]
Yong Liu[1]
Weigang Yuan[1]
Tan Yang[1]
Jia You[1]
Xingxing He[2]
Robert J Lee[3]
Lei Li[1]
Chuanrui Xu[1]

[1]School of Pharmacy, Tongji Medical College, Huazhong University of Science and Technology, [2]Institute of Liver Diseases, Tongji Hospital, Tongji Medical College, Huazhong University of Science and Technology, Wuhan, China; [3]Division of Pharmaceutics and Pharmaceutical Chemistry, College of Pharmacy, The Ohio State University, Columbus, Ohio, USA

Abstract: Multidrug resistance (MDR) due to overexpression of P-glycoprotein (P-gp) is a major obstacle that hinders the treatment of hepatocellular carcinoma (HCC). It has been shown that miR-375 inhibits P-gp expression via inhibition of astrocyte elevated gene-1 (AEG-1) expression in HCC, and induces apoptosis in HCC cells by targeting AEG-1 and YAP1. In this study, we prepared lipid-coated hollow mesoporous silica nanoparticles (LH) containing doxorubicin hydrochloride (DOX) and miR-375 (LHD/miR-375) to deliver the two agents into MDR HCC cells in vitro and in vivo. We found that LHD/miR-375 overcame drug efflux and delivered miR-375 and DOX into MDR HepG2/ADR cells or HCC tissues. MiR-375 delivered by LHD/miR-375 was taken up through phagocytosis and clathrin- and caveolae-mediated endocytosis. Following release from late endosomes, it repressed the expression of P-gp in HepG2/ADR cells. The synergistic effects of miR-375 and hollow mesoporous silica nanoparticles (HMSN) resulted in a profound increase in the uptake of DOX by the HCC cells and prevented HCC cell growth. Enhanced antitumor effects of LHD/miR-375 were also validated in HCC xenografts and primary tumors; however, no significant toxicity was observed. Mechanistic studies also revealed that miR-375 and DOX exerted a synergistic antitumor effect by promoting apoptosis. Our study illustrates that delivery of miR-375 using HMSN is a feasible approach to circumvent MDR in the management of HCC. It, therefore, merits further development for potential clinical application.

Keywords: hollow mesoporous silica nanoparticle, doxorubicin, miR-375, AEG-1, hepatocellular carcinoma, multidrug resistance

Introduction

Hepatocellular carcinoma (HCC) is among the most common solid tumor types and a leading cause of cancer-related death worldwide.[1] Treatment options for HCC are very limited and generally ineffective. Systemic chemotherapy is the most frequently used treatment for HCC because most patients are diagnosed with HCC at advanced stages when surgical treatment is no longer an option. Among the chemotherapeutic agents available for clinical treatment, doxorubicin hydrochloride (DOX) is most widely used either alone or in combination with other agents.

However, DOX-based chemotherapeutic options for HCC are often ineffective because of multidrug resistance (MDR). A known mechanism of MDR in cancer cells is the overexpression of ATP-binding cassette (ABC) transporter proteins, which pump out chemical agents and thus generate an MDR phenotype.[2–4] A well-studied

Correspondence: Chuanrui Xu; Lei Li
School of Pharmacy, Tongji Medical College, Hangkong Road 13, Wuhan, Hubei 430030, China
Tel +86 27 8369 2745
Email xcr@hust.edu.cn; leileilesure@163.com

submit your manuscript | www.dovepress.com
Dovepress
http://dx.doi.org/10.2147/IJN.S135306

ABC transporter is P-glycoprotein (P-gp) (also known as MDR1), which is overexpressed in MDR cells in many types of cancers, including pancreatic, breast, and colon cancers.[5–7] In HCC, MDR1 is also upregulated and shown to impede the effectiveness of chemotherapy.[8–10] Some studies have reported that MDR can be overcome by targeting MDR1.[11,12] In these studies, MDR1 siRNA was used for suppressing the expression of MDR1, which resulted in improved retention of chemotherapeutic agents in cancer cells.[10,13,14]

Our previous study showed that miR-375 can obstruct HCC progression in mice by suppressing yes-associated protein 1 (YAP1) and astrocyte elevated gene-1 (AEG-1).[15] Moreover, AEG-1 has been shown to play a pivotal role in chemoresistance in human HCC, neuroblastoma, and breast cancer.[15–18] In cancer cells, AEG-1 promotes the expression of MDR1, resulting in increased efflux and decreased accumulation of chemotherapeutics, which leads to drug resistance.[19,20] The molecular mechanism underlying this process includes facilitation of the association of MDR1 mRNA with polysomes by AEG-1, resulting in increased translation of MDR1 mRNA. AEG-1 also inhibits ubiquitination and subsequent proteasome-mediated degradation of the MDR1 protein.[19,21] Interestingly, miR-375 binds to the 3′ untranslated region of AEG-1 mRNA and blocks its translation through RNAi. Overexpression of miR-375 has been shown to inhibit AEG-1 and MDR1 expression in HCC cells.[18,22] As miR-375 is an endogenous miRNA that is downregulated in HCC, restoration of miR-375 may serve as a credible strategy to overcome MDR.

Nanovehicles, including liposomes, gold nanoparticles, polymeric micelles, and branched polymers, have shown great promise in the delivery of nucleotides.[23] In recent years, hollow mesoporous silica nanoparticles (HMSN) have emerged as an efficient tool for drug delivery because of their unique properties, such as large surface area, high pore volume, tunable pore size, and biocompatibility. In addition, they can be easily modified.[24–26] In addition, HMSN have been shown to effectively bypass the drug efflux activity of P-gp in MDR cancer cells.[27,28] However, due to negatively charged surface, it is not easy for HMSN to carry gene drugs including miRNAs, which are negatively charged as well. In contrast, cationic liposomes were widely used to deliver gene drugs through electrostatic adherence. Therefore, encapsulating the HMSN within the cationic lipid layer will enable it to carry both chemical drugs and gene drugs simultaneously. In addition, liposome fusion on HMSN cores can seal the cargo and thus prevent possible drug leakage. The liposome capsule also has an auxiliary role to facilitate transmembrane delivery of HMSN.

In this study, we prepared a lipid-coated HMSN (LH) formulation containing DOX and miR-375 (LHD/miR-375) and explored its efficiency to deliver miR-375 and DOX into MDR HCC cells. The synergistic antitumor effects of miR-375 and DOX were also studied. In addition, we investigated the intracellular trafficking, biodistribution, antitumor mechanism, and toxicity of LHD/miR-375 in mice.

Materials and methods

Materials

Doxorubicin hydrochloride (DOX), cetyltrimethylammonium chloride (CTAC; 25 wt%), tetraethylorthosilicate (TEOS), triethylamine (TEA), and paraformaldehyde (PFA) were purchased from Sigma Aldrich (St Louis, MO, USA). The 1,2-dioleoyl-3-trimethy-lammonium-propane (DOTAP, chloride salt) was purchased from Avanti Polar Lipids (Alabaster, AL, USA). Monomethoxy polyethylene was obtained from Acros Organics (Geel, Belgium). Monomethoxy polyethylene glycol 2000-distearoyl phosphatidylethanolamine (mPEG-DSPE2000) was obtained from Shanghai Advanced Vehicle Technology Ltd Co (Shanghai, China). Cholesterol (CHOL) was purchased from Acros Organics (Geel, Belgium). Cytochalasin, amiloride, dynasore, and genistein were purchased from Biotool (Shanghai, China). The sequence of miR-375 mimics used in this study was 5′-CCCGCGACGAGCCCCUCGCACA AAACGC-3′ and 5′-GCGUUUUGUUCGUUVGGCUC GCGUGAGG-3′. MiR-375 mimics were synthesized by Guangzhou Ribobio Company (Guangzhou, China). The negative control miR-NC was provided by Guangzhou Ribobio Company.

Preparation of HMSN and DOX loading

HMSN cores were synthesized according to the reported protocols with minor modification.[29] First, 35.7 mL of ethanol was mixed with 5 mL H_2O and 0.8 mL of ammonia and stirred for 5–10 min at room temperature to obtain uniform dense silica nanoparticles ($dSiO_2$). Then, 1 mL of TEOS was added and the mixture was allowed to react at room temperature for 1.5 h. Next, $dSiO_2$ nanoparticles were washed with H_2O and ethanol and suspended in 20 mL of water. Second, CTAC (2 g) and TEA (20 mg) were dissolved in 20 mL of deionized water and added to 10 mL of $dSiO_2$ aqueous solution. The mixture was stirred at room temperature for a prolonged period, followed by the addition of 0.15 mL TEOS. Then the mixture was stirred for 1 h at 80°C. Third, 636 mg of Na_2CO_3 was added to the reaction mixture, which was stirred continuously at 50°C for 1 h. Finally, CTAC was removed by NaCl:methanol extraction.[30]

To load DOX, HMSN (0.5 mg) was first suspended in 1 mg/mL of DOX solution. Ultrasonic processing was then performed for 5 min and the mixture was kept stirring for 24 h at room temperature in the dark. Subsequently, DOX-loaded HMSN (HD) was collected by centrifugation and washed with H_2O three times. The final concentration of HMSN was adjusted to 0.5 mg/mL in H_2O. To evaluate the DOX-loading efficiency, the supernatant was collected and the residual DOX content was determined using the calibration curve from a series of standard DOX solutions with an ultraviolet-visible spectrometer (756 PC; Shanghai Spectrum Instruments, Shanghai, China) at 480 nm. The amount of DOX loaded into the HD was calculated by subtracting the mass of DOX in the supernatant from the total mass in the initial solution. The loading capacity (LC) of DOX in the HD was calculated using the equation LC (%) = amount of DOX in the HD/weight of HD ×100%.

Preparation of lipid-coated HMSN/DOX and LHD/miR-375

Lipid-coated HD were synthesized as in the reported method.[31] Briefly, DOTAP, mPEG-DSPE2000, and CHOL at a molar ratio of 40:55:5 were dissolved in chloroform, and then lipid film formation was achieved by solvent evaporation over ~30 min using a rotary evaporator connected to a vacuum system at 45°C. The film was hydrated by adding 2 mL water with occasional shaking for 30 min at 60°C, forming a cloudy lipid suspension. A membrane with pore diameter of 200 and 100 nm was used and at least three extrusion cycles were performed. Clear liposomes were then obtained and stored in vials at 4°C. Equal volumes of the prepared HMSN and liposomes (5 mg/mL) were mixed by pipetting the mixture several times. The mixture was sonicated and allowed to sit at room temperature for 1 h with occasional agitation. Residual lipids were removed through centrifugation and the lipid coated HD (LHD) were dispersed in phosphate-buffered saline (PBS).

The LHD/miR-375 were prepared at a w/w (LHD/miRNA) ratio of 200:1 in RNase-free H_2O by adding stock solution of LHD into a prepared miRNA solution. The solution was then vortexed, and incubated at room temperature for 30 min to ensure miRNA loading efficiently.

Characterization of HMSN and LHD

The hydrodynamic diameter and zeta potential of HMSN and LHD suspended in PBS were measured by dynamic light scattering (DLS; Zeta Plus, Brookhaven Instruments, USA). The morphology of HMSN and LHD was observed by transmission electron microscope (TEM; JEOL JEM-1230, Tokyo, Japan) at an accelerating voltage of 200 keV. Nitrogen sorption isotherms were measured at 77 K with a Micromeritics ASAP2010 analyzer (Boynton Beach, FL, USA). Before measurements, the sample was dried in a vacuum oven at 373 K for 6 h, and outgassed in the instrument at 373 K to a residual pressure below 6.65×10^{-6} bar. The specific surface areas were calculated by the Brunauer–Emmett–Teller (BET) method in a linear relative pressure range between 0.05 and 0.25. The pore size distributions were derived from the desorption branches of the isotherms by the Barrett–Joyner–Halenda method using the Quantachrome Autosorb 1 software (Quantachrome Instruments, Boynton Beach, FL, USA).

In vitro DOX release

The release of DOX from LHD was performed using a dialysis method with pretreated dialysis bag.[32] Briefly, the LHD or HD solution (equivalent to 2 mg DOX) was put into a pretreated dialysis bag with 1/3 air gap and sealed with a dialysis bag holder. Then, the dialysis bag was dispersed in 30 mL 10 mM PBS at pH 7.4 and pH 5.0, respectively, and kept stirring under the dark. The concentration of DOX in PBS was detected with a UV spectrophotometer at 1, 3, 5, 6, 8, 12, 20, 24, 30, 48, and 72 h. At each time point, 1.0 mL of the external buffer was collected and replaced by 1.0 mL of fresh buffer.

Agarose gel electrophoresis

Agarose gel electrophoresis was used to evaluate miRNA loading in LHD. The miRNA or LHD/miR-375 (the dose of miRNA was 50 pmol) was applied to a 2% (w/v) agarose gel in Tris-acetate-EDTA (TAE) buffer containing Goldview staining reagent (Tianhang Biotech, Hangzhou, China). Free miRNA migrated in the gel while LHD/miR-375 were stuck in the loading wells. Images were obtained using a UV transilluminator and a digital imaging system (Life Science Technologies, MA, USA).

Cell culture and animals

HCC cell lines (HepG2, Hep3B, Huh7) and DOX-resistant HepG2 cells (HepG2/ADR) are all from the China Center for Type Culture Collection at Wuhan University (Wuhan, China). Cells were cultured with high-glucose Dulbecco's Modified Eagle's Medium (DMEM) supplemented with penicillin, streptomycin, and 10% fetal bovine serum (FBS) in 37°C and 5% CO_2 incubators. M-plasmocin (Invivogen, San Diego, CA, USA) at a concentration of 2.5 μg/mL was used to prevent the possible mycoplasma infections.

FVB/N and BALB/c nude mice were purchased from Beijing HFK Bioscience (Beijing, China) and kept in filter-topped

cages with standard rodent chow, water available ad libitum, and a 12-h light/dark cycle. Animal experiments were performed according to national regulations, Regulations for the Administration of Affairs Concerning Experimental Animals in China, and approved by the Committee on Ethical Animal Experiment at Huazhong University of Science and Technology.

Uptake, drug accumulation, and intracellular track of LHD/miR-375

To visualize the extent of cellular uptake, HepG2 or HepG2/ADR cells were seeded on a 12-well plate at 1×10^5 cells per well and cultured overnight. LHD/miR-375 or free DOX were then added to the medium for different times (0.5, 1, 2, and 6 h) at an equivalent DOX concentration of 5 μg/mL or 50 nM miRNA. For drug accumulation and retention experiments, cells were incubated with LHD or DOX for 4 h, washed twice with PBS, replenished with fresh DMEM, and continued to incubate for another 24 h. After treatment with drugs, cells were washed with PBS three times and then fixed with 4% PFA. Solution of 4,6-diamidino-2-phenylindole (DAPI) (Thermo Fisher Scientific, Waltham, MA, USA) was used for staining of the nucleus. Stained cells were observed with fluorescence microscope (Olympus, Tokyo, Japan). To determine intracellular fluorescence intensity of DOX, cells were trypsinized, washed, and resuspended in 200 μL of PBS and then measured using a flow cytometer (Becton Dickinson, San Jose, CA, USA).

For determination of the intracellular fate of LH/miR-375, HepG2/ADR cells were seeded in a 15-mm FluoroDish (NEST, Wuxi, China) and incubated with LH/miR-375 (Cy3-labeled miR-375) in complete DMEM for different time points. Cells were then rinsed with PBS, fixed in 4% PFA for 15 min, and permeated with 0.1% Triton X-100 for 3 min. After blocking with 5% goat serum in PBS for 30 min, cells were incubated with a primary antibody against the proteins of interest at 1:200 in goat serum, overnight at 4°C. Next, cells were rinsed three times with PBS and then incubated with an AlexaFluor 488-labeled secondary antibody (Alexa Fluor 488 Goat Anti-Rabbit IgG [H+L]; Thermo Fisher Scientific) at 1:200 in goat serum for 45 min at room temperature. Then, the cells were imaged under a Zeiss LSM 700 inverted confocal scanning microscope. The primary antibodies include EEA1 (Cell signaling #3288), Rab9 (Cell signaling #5118), LAMP1 (Cell signaling #9091), and Giantin (Proteintech 2804).

Internalization mechanism of LHD

To evaluate the endocytic pathway of LHD, HepG2/ADR cells were pretreated with cytochalasin (10/20 μM), amiloride (10/20 μM), dynasore (10/20 μM), or genistein (100/200 μM) for 30 min, followed by incubation with LHD (2.5 μg/mL DOX) for 2 h. Then cells were trypsinized, washed with PBS, and resuspended for flow cytometry detection. LHD-positive cells were detected through the fluorescence of DOX.

Cell proliferation analysis

The cytotoxic effects of LHD/miR-375 on HCC cells were measured using a Cell Counting Kit-8 kit (CCK-8 kit; Dojindo Laboratories, Kumamoto, Japan). The cells were seeded onto 96-well plates with 8,000 cells in each well. After 12 h, cells were treated with DOX, LHD, or LHD/miR-375 at a series of concentrations. After incubation for an additional 48 h, the portions of viable cells were measured using CCK-8 kit according to the user's manual. Cell viability within each group was expressed as a percentage of the viability of untreated control cells.

Detection of mitochondrial membrane potential

HepG2/ADR cells were seeded on a 12-well plate at 1×10^5 cells per well and cultured overnight. Cells were treated with 0.25 μg/mL DOX or 100 nM miR-375 for 24 h. Mitochondrial membrane permeability was detected in a flow cytometer after the cells were treated with the Mitochondrial Permeability Detection Kit (Beyotime, Wuhan, China). The lipophilic dye JC-1 in this kit can enter the mitochondria and emit green fluorescence in low mitochondrial potential as monomer or emit red fluorescence in high mitochondrial potential as aggregates.

Western blot analysis

HepG2 and HepG2/ADR cells were harvested after 48 h treatment and lysed using RIPA buffer (R0278; Sigma Aldrich, St Louis, MO, USA). The lysates were centrifuged and the supernatant was collected for Western blotting as the routine protocol. The following antibodies were used: anti-AEG-1 (1:2,000; ProteinTech, IL, USA), anti-YAP1 (1:1,000; Cell signaling, MA, USA), anti-Bcl-2 (1:1,000; Cell signaling, USA), anti-cleaved-caspase-3 (1:1,000; Cell signaling, USA), anti-caspase-3 (1:1,000; Cell signaling, USA), anti-Bax (1:1,000; Cell signaling, USA), anti-P-gp (1:1,000; Abcam, Cambridge, UK), and anti-α-tubulin (1:1,000; Promoter, Wuhan, China).

Drug distribution in mice

For the tissue distribution assay, subcutaneous HepG2/ADR tumors were implanted by inoculating 5×10^6 HepG2 cells in the front armpit of the female BALB/c nude mice (6–8 weeks

of age, 16–18 g). When tumors grew to 500 mm^3, LHD or free DOX was injected via the lateral tail vein at 8 mg/kg DOX. At different time points after the injection (0.5, 1, 2, 4, 8, 12, and 24 h), 500 µL blood was collected in heparin-treated tubes and then centrifuged (5,000 rpm, 5 min) at room temperature to obtain plasma. Plasma aliquots of 100 µL were added with 100 µL ethanol, 20 µL deionized water, and 5 µL 20% sodium dodecyl sulfate, and then were vortexed 30 s and centrifuged (12,000× *g*, 10 min) at 4°C to extract the DOX from the plasma protein. Mouse lungs, hearts, livers, spleens, kidneys, and tumor tissues were also collected. Tissues of 0.1 mg were homogenized with the buffer (60% EtOH, 0.3 mol/L HCl, and 40% H_2O), and then centrifuged (Eppendorf 5415D, 12,000 rpm, 15 min) at 4°C to collect the supernatant. The concentration of DOX was determined by fluorescence spectrophotometer (HitachiF-2700; software FL solution, Tokyo, Japan). For in vivo imaging, mice were killed and organs were collected for ex vivo tissue imaging (Bruker In-vivo FX Pro; Bruker, CA, USA) 1, 6 and 12 h following injection.

Antitumor effects of LHD/miR-375 in xenograft and primary tumor model

For antitumor efficacy study in the xenograft tumor model, mice were randomly divided into five groups (n=6) when tumor volume reached ~100 mm^3. Saline, DOX, LH/miR-375, LHD, or LHD/miR-375 were injected via tail vein at 6 mg/kg DOX and/or 4 nmol/kg miR-375 three times on days 10, 16, and 22 after HepG2/ADR cell inoculation. Tumor sizes and mouse weights were measured every 3 days. At the end of the experiment, mice were killed and tumors were collected and photographed. The tumor size was calculated by the equation V = length × $width^2$ ×0.52.

For the primary tumor model, wild-type FVB/N mice at age of 6–8 weeks and with body weights at 18–20 g were used. The hyperactive transposase construct pCMV/SB, Ras gene construct pCaggs-RasV12, and Akt gene construct myr-Akt/pT3EF1α were obtained from Dr Xin Chen at University of California at San Francisco, USA. The plasmids were extracted and purified with a GenElute Endotoxin-free plasmid Maxiprep Kit (Sigma, USA) before being injected into mice. Hydrodynamic injections were performed as reported previously.[33,34] In brief, FVB/N mice were injected with 5 µg myr-Akt/pT3EF1α, 5 µg NRasV12/pT2-Caggs, and 0.4 µg pCMV/SB in 2 mL saline via tail vein in 5–10 s. Upon injection, the Ras and Akt plasmid, along with transposase plasmid were taken up by hepatocytes and integrated into their chromosomes. The continuous overexpression of Ras and Akt induced the formation of tumor in the liver. The tumors were monitored by bimanual palpation for ballooning and stiffness of livers and confirmed by dissection before drug administration. Tumors were generally formed in mice 3 weeks after Akt/Ras injection. Then mice were given tail vein injections of saline, DOX, LH/miR-375, LHD, or LHD/miR-375 (6 mg/kg DOX or 4 nmol/kg miR-375) every other day for a total of 2 weeks accompanied by body weight measurement. Subsequently, the mice were killed and the livers were photographed and examined. Tumor tissues were also collected and fixed in 4% PFA, embedded in paraffin, cut into 4 micrometers and mounted on polylysine-coated slides. Then, hematoxylin and eosin, immunohistochemistry, and terminal deoxynucleotidyl transferase dUTP nick end labeling (TUNEL) staining were performed on those slides according to routine protocols.

Statistical analysis

Comparison of two groups was performed using the Student's *t*-test (SPSS Software, Chicago, IL, USA). Multiple groups were compared by one-way analysis of variance followed with Dunnett's post-test. A value of $P<0.05$ was considered significant.

Results and discussion

Preparation and characterization of LHD/miR-375

The procedure used to prepare the LHD/miR-375 has been summarized in Figure 1. Briefly, HMSN cores were synthesized using a modified Stöber method.[30] Next, DOX was incorporated into the HMSN by constant stirring. We measured the loading efficiency of DOX in HMSN and found that the maximum DOX loading was 1.12 mg/mg (DOX:HMSN). To deliver miR-375 and prevent premature leakage of DOX, the HMSN were then packaged into a lipid bilayer through fusion with cationic liposomes. TEM showed that the HMSN had uniform spherical shapes (Figure 2A). The BET surface area, pore volume, and pore size of HMSN were calculated to be 358 m^2/g, 0.30 cm^3/g, and 3.5 nm, respectively. The sharp pore size distribution of HMSN indicates a uniform mesoporous structure, consistent with the TEM imaging of HMSN (Figure 2B). After being coated with lipid bilayer, LHD also showed a uniform spherical shape and even lipid bilayer with an average thickness of 5 nm (Figure 2C). DLS analysis showed that the average particle size of the LHD was 210 nm, which was 18 nm larger than that of the HMSN cores (Table 1). In addition, the HMSN were negatively charged (–32 mV), whereas the LHD were positively charged (+27 mV) (Table 1). The positive charge of the LHD was attributed to the cationic lipid coating, which covered the

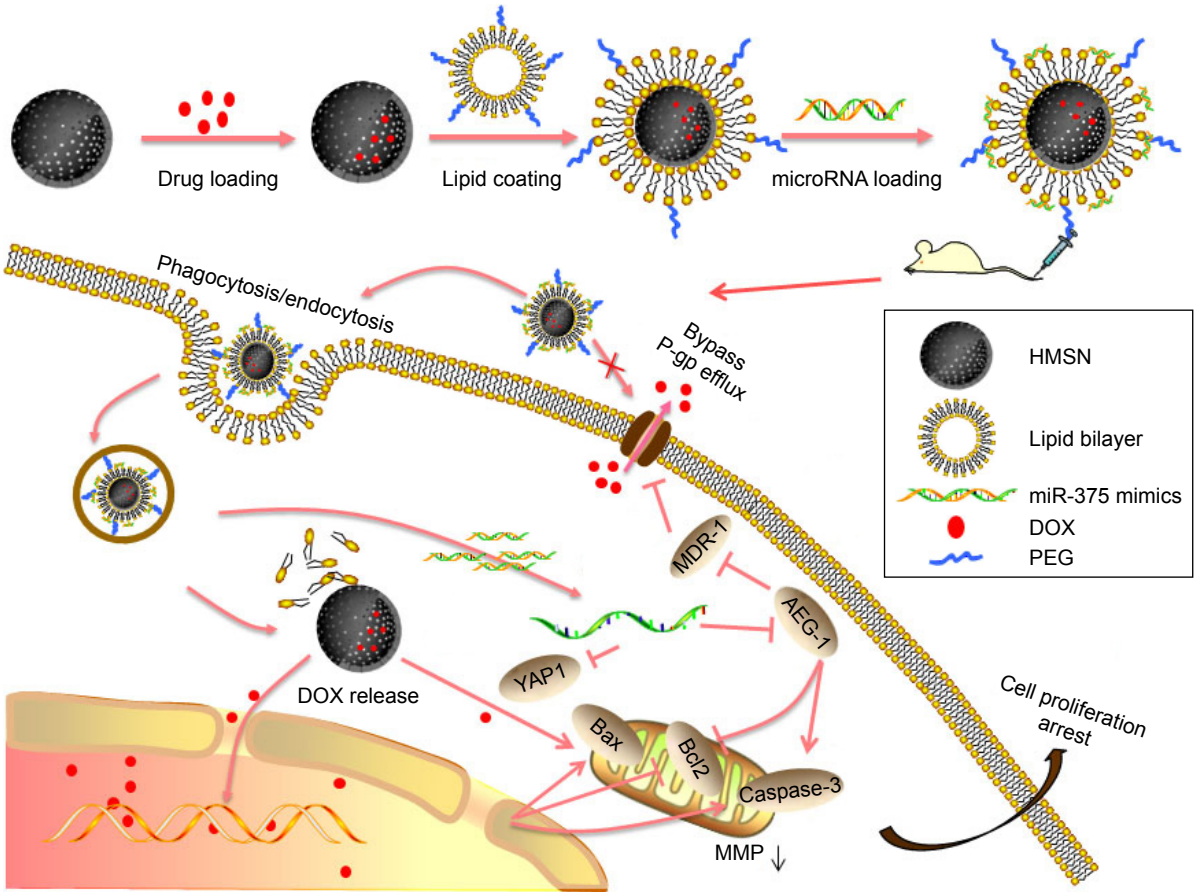

Figure 1 Schematic illustration of drug loading, cellular entry, drug release, and antitumor mechanism of LHD/miR-375.
Abbreviations: DOX, doxorubicin hydrochloride; HMSN, hollow mesoporous silica nanoparticles; LHD, lipid-coated hollow mesoporous silica nanoparticles containing doxorubicin hydrochloride; MDR, multidrug resistance; MMP, mitochondrial membrane potential; PEG, polyethylene glycol; P-gp, P-glycoprotein.

negatively charged silicon on the surfaces of the HMSN. Furthermore, the LHD/miR-375 were found to be hydrated particles with an average size of 262 nm and a zeta potential of 12 mV. The size and zeta potential of the LHD/miR-375 were larger and lower, respectively, than the respective values obtained for the LH because of the incorporation of miR-375 (Table 1).

The microenvironment of tumor tissues tends to be more acidic (pH 5.0–6.5) than that of normal tissues (pH 7.4); therefore, we examined the release properties of DOX from

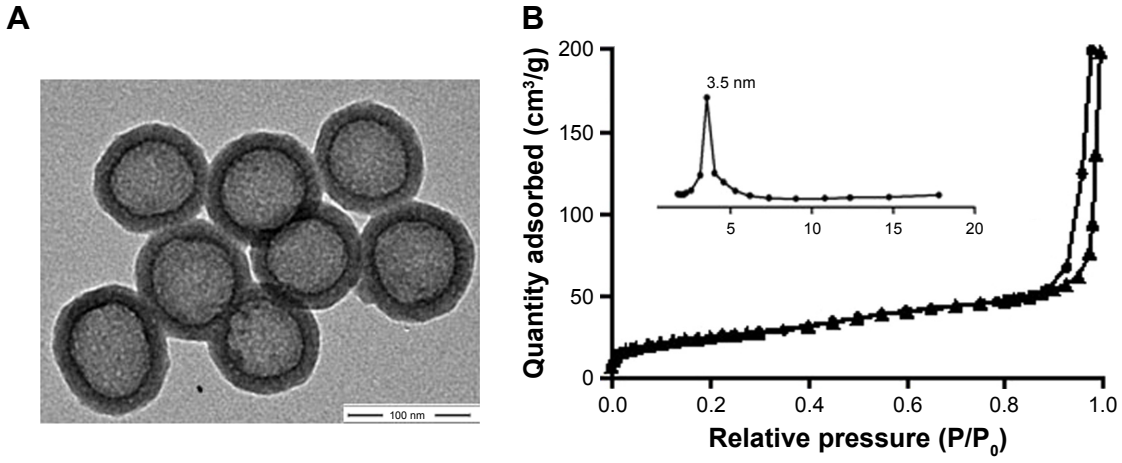

Figure 2 (*Continued*)

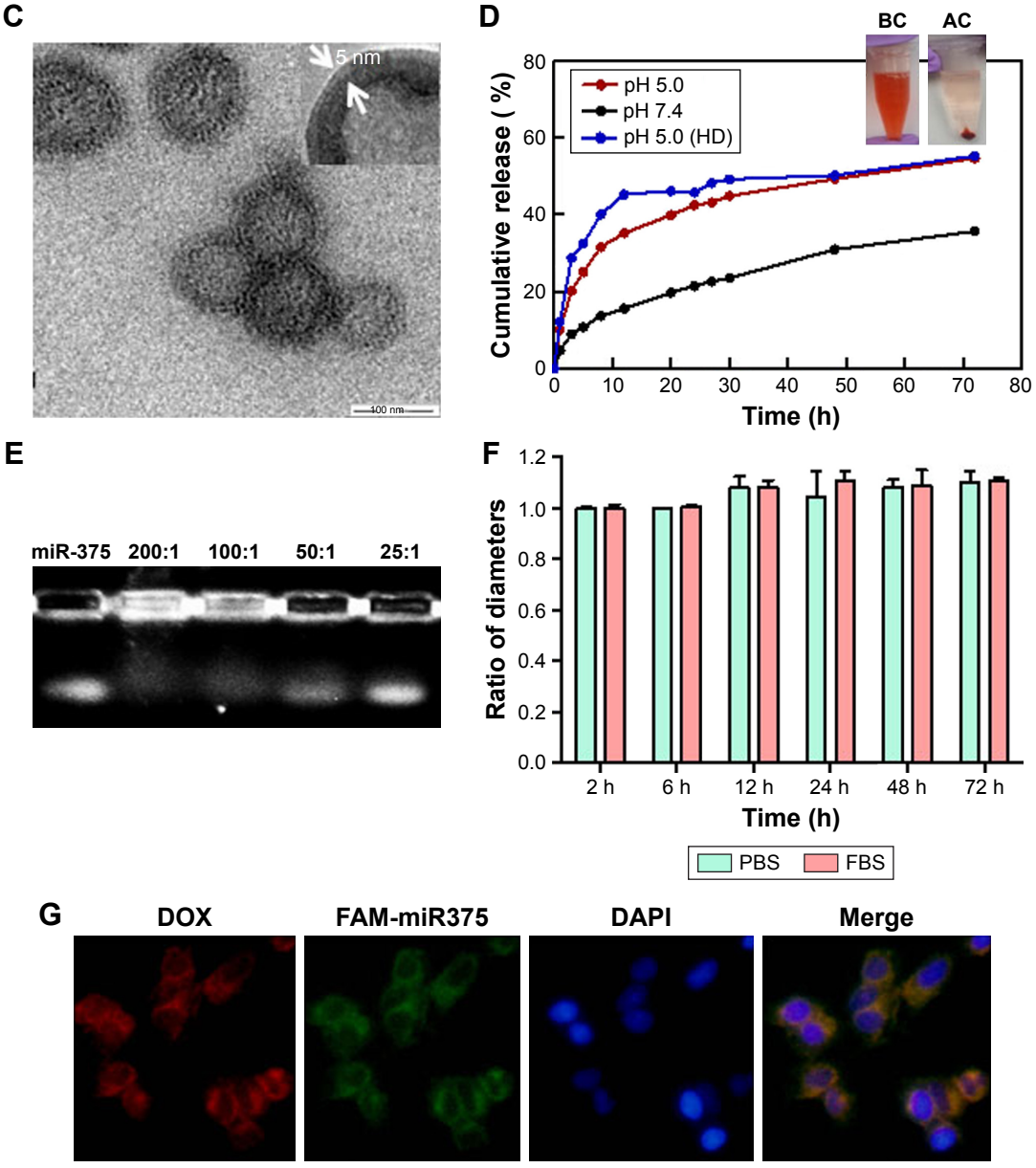

Figure 2 Characterization of LHD/miR-375.

Notes: (**A**) TEM images of HMSN. (**B**) Nitrogen sorption isotherms and corresponding pore size distributions of HMSN samples. (**C**) TEM images of LHD. (**D**) Release of DOX from the LHD (at pH 5.0 and 7.4) and HD (at pH 5.0). Pictures of LHD solution before (BC) and after (AC) centrifugation were illustrated. (**E**) Detection of miR-375 loading efficiency by agarose gel electrophoresis at LHD/miR-375 ratios from 25:1 to 200:1 (w/w). (**F**) Time-dependent stability of LHD in PBS and FBS at 37°C. (**G**) Cellular uptake of LHD/miR-375 and intracellular distribution of DOX and miR-375 in HepG2 cells after 1 h incubation.

Abbreviations: DAPI, 4′,6-diamidino-2-phenylindole; DOX, doxorubicin hydrochloride; FBS, fetal bovine serum; HD, HMSN loaded with doxorubicin hydrochloride; HMSN, hollow mesoporous silica nanoparticles; LHD, lipid-coated hollow mesoporous silica nanoparticles containing doxorubicin hydrochloride; PBS, phosphate-buffered saline; TEM, transmission electron microscope.

Table 1 Characterization of nanoparticles by dynamic light scattering detection (n=3)

Groups	Particles size (nm)	Polydispersity	Zeta potential (mV)
Hollow mesoporous silica nanoparticles	192±2.6	0.005±0	−32±5.7
LHD	210±1.3	0.071±0.048	+27±8.1
LHD/miR-375	262±13.4	0.254±0.03	+12±9.3

Note: Data presented as mean ± standard deviation.

Abbreviation: LHD, lipid-coated hollow mesoporous silica nanoparticles containing doxorubicin hydrochloride.

the LHD in PBS and at a lower pH. As shown in Figure 2D, the release of DOX from the LHD at pH 5.0 was more rapid and efficient than that at pH 7.4, suggesting an acid-labile release property of LHD. Furthermore, the LHD showed a slower release of DOX than the DOX-loaded HMSN (HD) did, which indicates that the lipid bilayer decreased the premature release of DOX (Figure 2D). Centrifugation of the LHD suspension led to precipitation of DOX, which suggested that the HMSN were loaded with DOX (Figure 2D). Maximum

miR-375 loading was achieved at an LHD:miR-375 ratio of 200:1 (w/w, Figure 2E). Stability of the LHD/miR-375 was assessed at a physiological pH of 7.4, which was simulated using PBS and FBS at 37°C. After 3 days of incubation, no significant changes in the size of the LHD/miR-375 were observed in either medium (Figure 2F).

To investigate whether LHD/miR-375 could deliver DOX and miR-375 simultaneously into cells, we incubated HepG2 cells with LHD/miR-375 for 1 h. We found that both DOX and miR-375 were present at the perinuclear regions of the cytoplasm (Figure 2G), indicating that the cationic lipid-coated LHD are capable of co-delivering miR-375 and DOX into HCC cells.

Uptake of LHD and LHD/miR-375 by HepG2/ADR cells

To further evaluate the uptake efficiency and retention of the LHD in MDR HCC cells, we treated HepG2 and HepG2/ADR cells with DOX or LHD (Figure 3A) and observed for 6 h. In HepG2 cells, free DOX passed through the cell membrane and subsequently entered into the nucleus at 0.5 h following treatment. However, no DOX was observed in HepG2/ADR cells at 0.5 h, and only small amounts of DOX were observed in a few of HepG2/ADR cells before the end of 6 h. In contrast, the LHD were found in the cytoplasm in both HepG2 and HepG2/ADR cells at 0.5 h. Furthermore, at 6 h, a large amount of DOX was found released from the LHD and had accumulated in the cytoplasm in HepG2/ADR cells.

Quantitative analysis by flow cytometry showed that the uptake efficiencies of LHD and free DOX by the HepG2 cells were comparable; however, uptake of the LHD was 1.5- to 2.5-fold higher than that of free DOX in HepG2/ADR cells (Figure 3B). Drug efflux analysis in HepG2 cells showed that no significant efflux of free DOX, LHD, or LHD/miR-375 occurred after treatment of the cells with the respective formulations (Figure 3C and D). However, most of the DOX (~80%) was pumped out of HepG2/ADR cells after treatment with free DOX. In the HepG2/ADR cells that were treated with LHD or LHD/miR-375, efflux of DOX was found to be 32% and 28%, respectively. As a control treatment, verapamil (a P-gp inhibitor) reduced DOX efflux to 61.5% (Figure 3C and D). Interestingly, P-gp levels in the cells were significantly increased by DOX but decreased by LHD/miR-375 (Figure 3E and F). Together, these results indicate that the LHD promote the uptake and accumulation of DOX in HepG2/ADR cells. In addition, the LHD/miR-375 potentially enhanced this effect by repressing P-gp expression.

Endocytic mechanism and intracellular fate of LHD/miR-375

To explore how the LHD promoted the uptake of DOX and reduced its efflux, we investigated the endocytic pathway of LHD using various endocytosis inhibitors. We found that the uptake of LHD by HepG2/ADR cells was effectively blocked in a dose-dependent manner by amiloride (inhibitors of phagocytosis), dynasore (inhibitor of clathrin-mediated endocytosis), and genistein (inhibitor of clathrin- and caveolae-mediated endocytosis) in a dose-dependent manner; however, the process was not blocked by cytochalasin D (inhibitor of macropinocytosis) (Figure 4A). This result indicates that the LHD were taken up by the tumor cells mainly through phagocytosis, and clathrin- and caveolae-mediated endocytosis.

Next, we examined the localization of Cy3-labeled LH/miR-375 in HepG2/ADR cells using a confocal microscope (Figure 4B). At 1 h post-treatment, most of the LH/miR-375 had adhered to the cell membranes and were entrapped in early endosomes. At 4 h, the majority of the LH/miR-375 were found in late endosomes. After 8 h, most of the LH/miR-375 were retained in late endosomes, whereas some LH/miR-375 entered lysosomes. At 16 h, miR-375 was found dispersed in cytoplasm, which indicated the escape of the LH/miR-375 from the endosomes and the subsequent release of miR-375 from LH/miR-375 particles. Moreover, we did not observe an appreciable colocalization of LH/miR-375 or miR-375 and the trans-Golgi network. Significantly, the escape of the LH/miR-375 from the endosomes could avoid the degradation of miR-375 in the lysosomes or Golgi complex. In addition, release of miR-375 in late endosomes also suggests that DOX was released mainly in late endosomes or lysosomes because encapsulated DOX ought to escape after miR-375 release when the lipid capsule is degraded. Furthermore, release of DOX from late endosome or lysosomes may reduce the binding of DOX to P-gp. This decreases the efflux of DOX because late endosomes and lysosomes are spatially closer to the nucleus rather than the cellular membrane, which is where P-gp proteins are located. Subsequently, released DOX is capable of entering the nucleus instead of being pumped out.

In vitro cytotoxic activity of LHD/miR-375

We evaluated the cytotoxic effects of various miR-375 and DOX formulations in HepG2, Huh7, Hep3B, and HepG2/ADR cells (Figure 5A). After 48 h of treatment, it was observed that the cytotoxicity of the LHD was not significantly higher than that of DOX against HepG2,

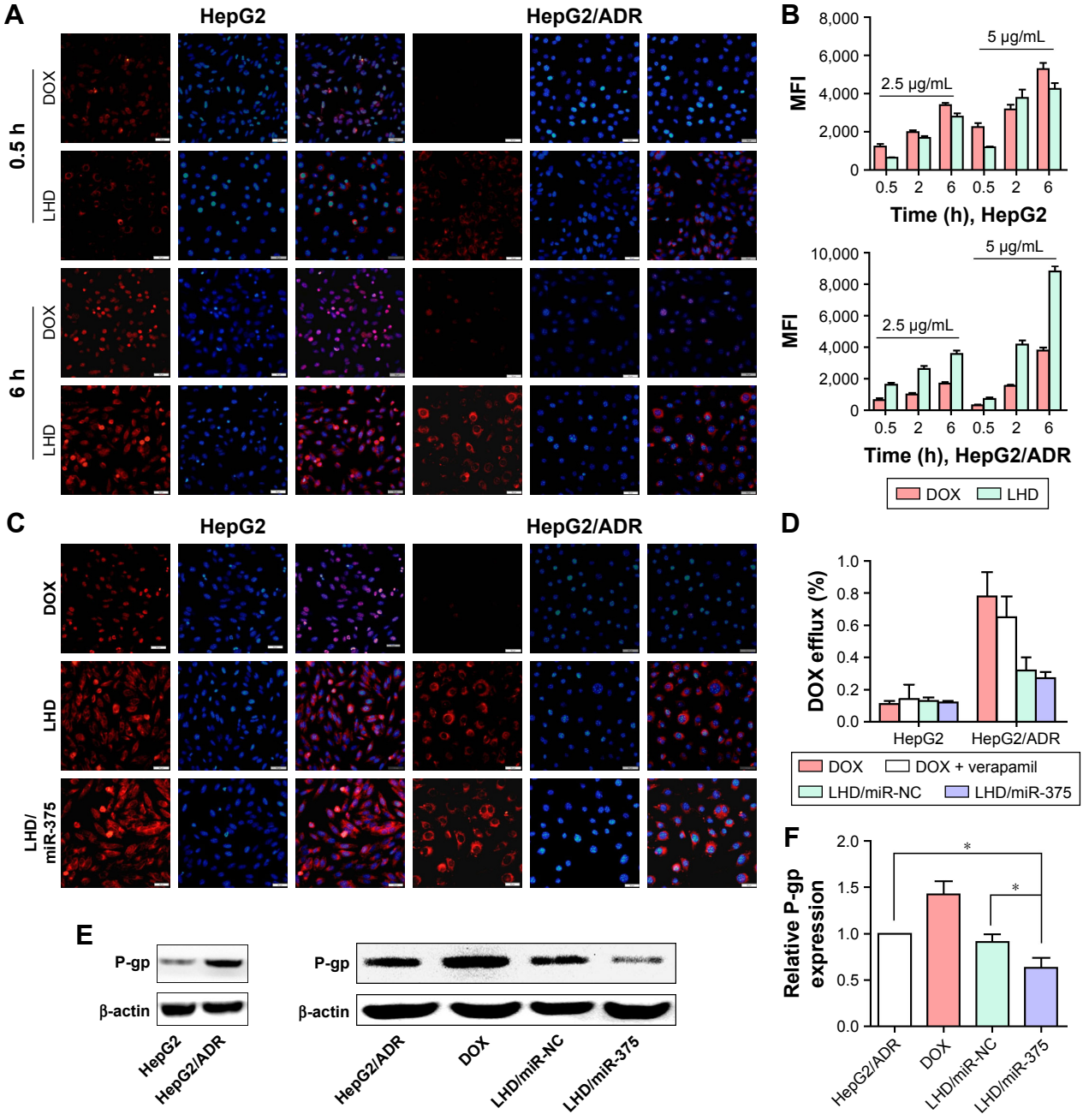

Figure 3 Uptake and retention of LHD in HepG2 and HepG2/ADR cells.

Notes: (**A**) Uptake of LHD in HepG2 and HepG2/ADR cells determined by fluorescence microscopy. Cells were incubated with DOX (5 μg/mL) or LHD (5 μg/mL). (**B**) Uptake of LHD in HepG2 and HepG2/ADR cells determined by flow cytometry. Cells were incubated with DOX (2.5 or 5 μg/mL) or LHD (2.5 or 5 μg/mL). (**C**) Retention of LHD/miR-375 in HepG2 and HepG2/ADR cells determined by fluorescence microscopy. HepG2 and HepG2/ADR cells were incubated with DOX (5 μg/mL), LHD (5 μg/mL DOX), or LHD/miR-375 (5 μg/mL DOX and 100 nM miR-375) for 4 h and then cultured with medium without drugs for another 24 h. (**D**) DOX efflux determined by flow cytometry. HepG2 and HepG2/ADR cells were treated with DOX (5 μg/mL), DOX + verapamil (DOX 5 μg/mL and verapamil 10 μM), LHD/miR-NC (DOX 5 μg/mL and 100 nM miR-NC), or LHD/miR-375 (5 μg/mL DOX and 100 nM miR-375). The nuclei were counterstained by 4,6-diamidino-2-phenylindole. (**E**) Western blotting assay for P-gp protein expression after DOX, LHD/miR-NC, or LHD/miR-375 treatment in HepG2/ADR cells. (**F**) P-gp protein level by quantifying the Western blotting bands. P-gp level in untreated cells was standardized to 1. Data are expressed as mean ± standard error of the mean of three independent experiments. *$P<0.05$.

Abbreviations: DOX, doxorubicin hydrochloride; LHD, lipid-coated hollow mesoporous silica nanoparticles containing doxorubicin hydrochloride; P-gp, P-glycoprotein; MFI, mean fluorescence intensity; NC, negative control.

Hep3B, and Huh7 cells; however, the LHD/miR-375 were more cytotoxic against the cells than the LHD or DOX were. Furthermore, after 48 h of treatment, LHD and LHD/miR-375 showed higher antitumor activities in HepG2/ADR cells than DOX did; however, the LHD/miR-375 showed a higher activity than the LHD did. These results indicate that LHD can exert anti-MDR effects in HepG2/ADR cells. Additionally, the anti-MDR effect was enhanced by the miR-375 in the LHD/miR-375 as was expected. Moreover, IC_{50} analysis also showed that antitumor activity

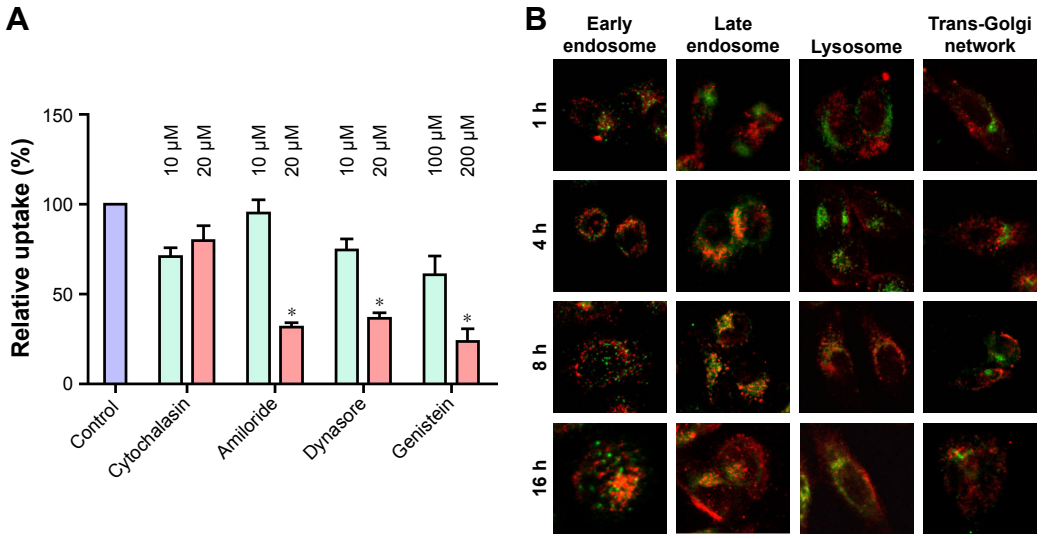

Figure 4 Endocytic pathway and subcellular localization of LHD.

Notes: (**A**) Inhibition of the uptake of LHD in HepG2/ADR cells using specific endocytosis inhibitors. HepG2/ADR cells were cultured with inhibitors for 0.5 h and then treated with LHD (2.5 μg/mL) for 2 h. Data are expressed as mean ± standard error of the mean of three independent experiments. Uptake in cells without inhibitor treatment but with LHD treatment was used as control and normalized to 100%. (**B**) Confocal microscopic images of HepG2/ADR cells after culturing with LH/miR-375 (50 nM miR-375). MiR-375 was labeled with Cy3 (red); early endosome, late endosome, lysosome, and trans-Golgi network were stained as green. The magnification of each image is 400×. *$P<0.05$.

Abbreviation: LHD, lipid-coated hollow mesoporous silica nanoparticles containing doxorubicin hydrochloride.

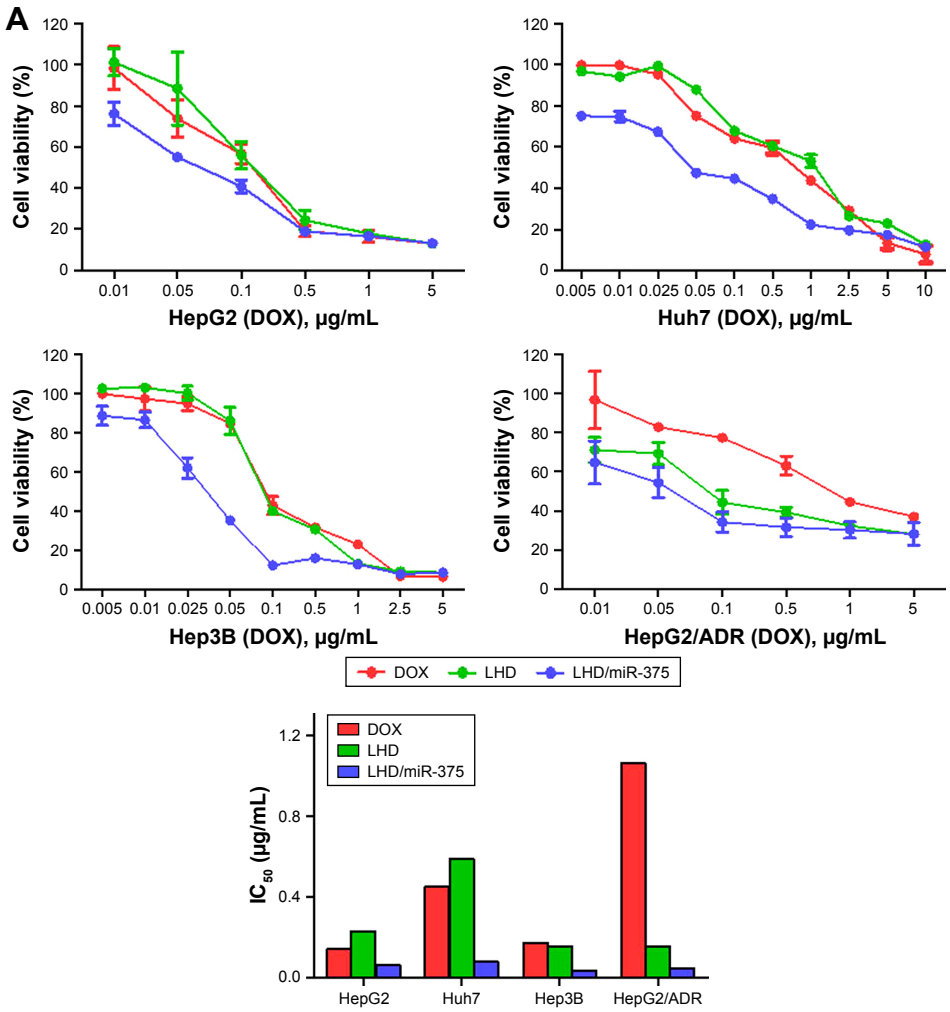

Figure 5 (*Continued*)

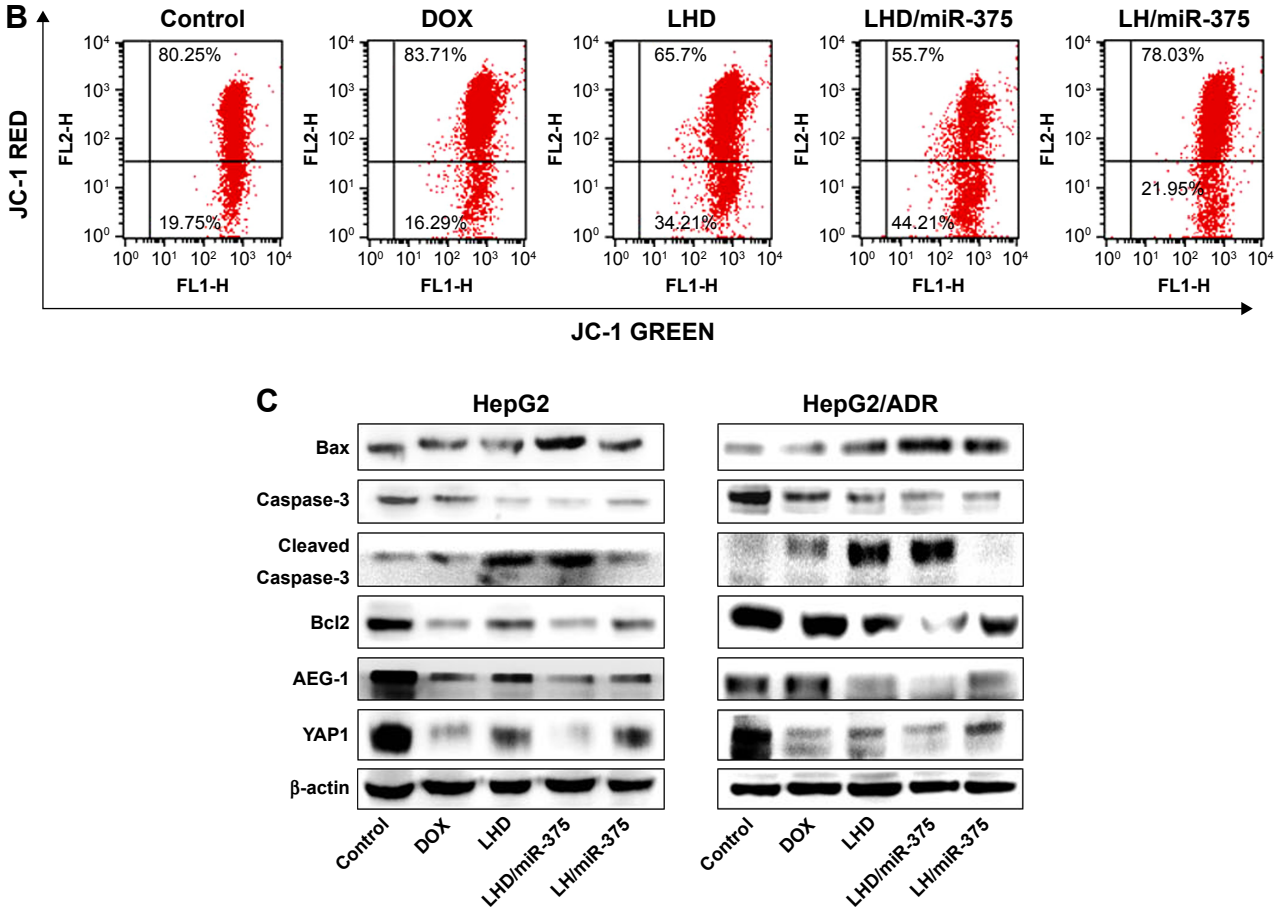

Figure 5 Antitumor activity of LHD/miR-375 in HCC cell lines.

Notes: (**A**) Viability of HepG2, Huh7, Hep3B, and HepG2/ADR cells after treatment, and IC_{50} of DOX, LHD, and LHD/miR-375 in those cells. Cells were treated with drugs at indicated concentrations of DOX for 48 h. Cell viability was determined by MTT assay, and viabilities of untreated cells after 48 h culture were used as control and normalized as 100%. (**B**) MMP detection in HepG2/ADR cells after 24 h drug treatment followed by flow cytometry analysis. (**C**) Western blotting of apoptotic-related and miR-375 target proteins in HepG2 and HepG2/ADR cells after treatment with drugs. Cells were treated with drugs for 48 h and then harvested for Western blotting. β-actin was used as loading control.

Abbreviations: DOX, doxorubicin hydrochloride; HCC, hepatocellular carcinoma; LH, lipid-coated hollow mesoporous silica nanoparticles; LHD, lipid-coated hollow mesoporous silica nanoparticles containing doxorubicin hydrochloride; MMP, mitochondrial membrane potential.

was greatly enhanced by the incorporation of miR-375 into LHD, demonstrating a synergistic co-efficiency between DOX and miR-375 (Figure 5A).

DOX is reported to kill tumor cells by inducing apoptosis and loss of mitochondrial membrane integrity, which is an early event in apoptotic signaling.[35] Subsequently, the damaged mitochondrial membrane causes a decrease in mitochondrial membrane potential (MMP). Therefore, we determined the effect of the LHD/miR-375 on MMP using a JC-1 kit. In the mitochondria, JC-1 aggregates when MMP decreases. The results obtained showed that the treatment with DOX produced only 16.29% JC-1 aggregates, whereas that with the LHD significantly increased the amount of green fluorescent JC-1 aggregates to 34.21%. The LHD/miR-375 further increased the quantity of JC-1 aggregates to 44.21% (Figure 5B). These results indicate that increased DOX uptake by the cells promoted mitochondrial depolarization in the tumor cells and miR-375 also contributed to mitochondria-primed apoptosis.

We also determined the effects of the LHD and LHD/miR-375 on the expression levels of apoptosis-related genes in HepG2 and HepG2/ADR cells (Figure 5C). In HepG2 cells, the LHD formulation did not increase the expression of cleaved caspase-3 and Bax, or decrease Bcl2 expression. Nevertheless, the LHD/miR-375 significantly increased the expression of Bax and cleaved caspase-3, and decreased the expression of Bcl2. In HepG2/ADR cells, however, the LHD significantly increased the expression of Bax and cleaved caspase-3, and decreased Bcl2 expression. In addition, the LHD/miR-375 enhanced the effect of the LHD. Moreover, both the LHD/miR-375 and the LH/miR-375 inhibited the expression of AEG-1 and YAP1 in HepG2 and HepG2/ADR cells, which suggests that exogenous miR-375 delivered by the LHD/miR-375 functioned

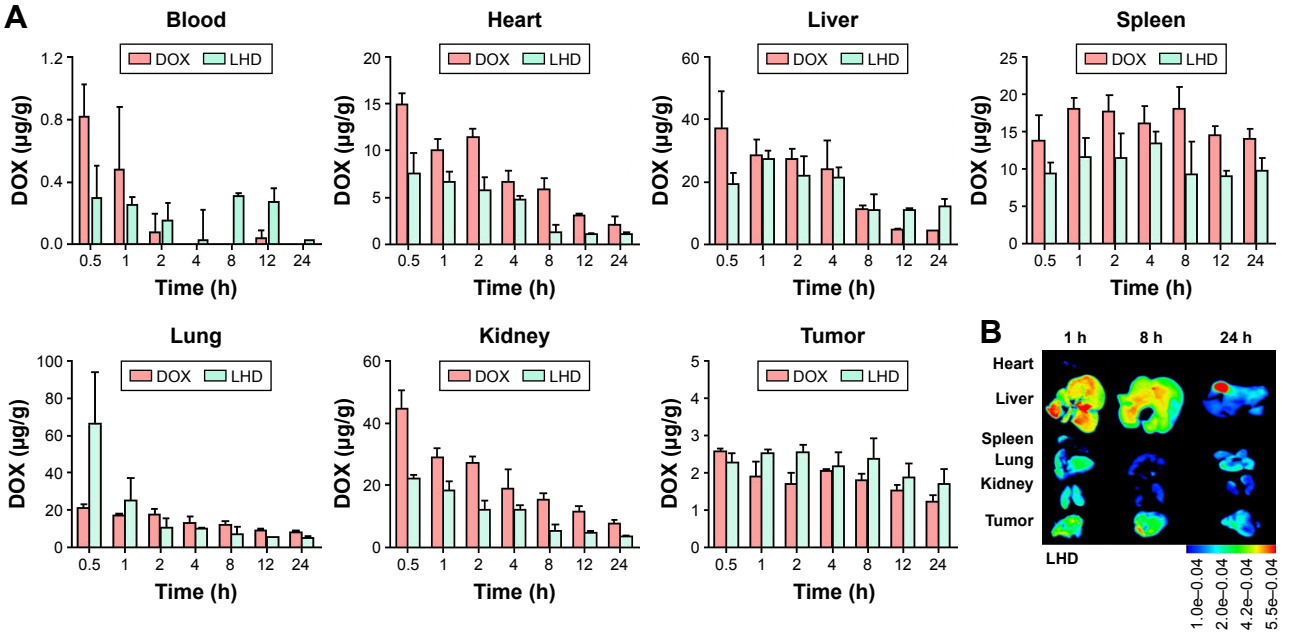

Figure 6 DOX distribution followed administration of DOX or LHD in xenograft tumor mice.
Notes: (**A**) Tissue distribution and blood concentration of DOX at 0.5, 1, 2, 4, 8, 12, and 24 h after a single intravenous injection of DOX (8 mg/kg) or LHD (8 mg/kg DOX) in mice. DOX concentrations were determined using a fluorescence spectrometer and calculated using a standard curve. (**B**) Images of LHD distribution in mouse tissues. Data are expressed as mean ± standard error of the mean of three samples.
Abbreviations: DOX, doxorubicin hydrochloride; LHD, lipid-coated hollow mesoporous silica nanoparticles containing doxorubicin hydrochloride.

as endogenous miR-375. These results further indicate that the LHD enhanced the antitumor effect of DOX in HepG2/ADR cells. Additionally, miR-375 and LHD have a synergistic effect.

Distribution of the LHD in mouse tissues

To determine the distribution of the LHD in mouse tissues, we injected tumor-bearing BALB/c nude mice with the formulation and examined the distribution of DOX using a fluorescence spectrophotometer. In peripheral circulation, DOX was quickly cleared after 4 h while LHD significantly prolonged the circulation time (Figure 6A). Besides, it was observed that the amounts of DOX that had accumulated in the hearts, lungs, spleens, and kidneys of the mice from the LHD injections were significantly lower than those from the free DOX injections (Figure 6A). However, the LHD injections led to higher DOX accumulation in the mouse livers and tumors than the free DOX injection did (Figure 6A), suggesting that the LHD increased DOX distribution in the tumor tissues but decreased its distribution in normal tissues. As a result, the side effects of DOX in the normal organs, especially injury to the heart, may be reduced. The high accumulation of DOX from the LHD injection in the tumor tissues favors the use of the formulation as an antitumor agent, and the high accumulation in the liver may be favorable in HCC treatment. Observation of isolated organs with the in vivo imaging system confirmed that DOX was mainly accumulated in liver and tumor tissues, which is consistent with the quantitative analysis (Figure 6B).

LHD/miR-375 suppressed tumor growth in mice

To determine the antitumor effect of LHD/miR-375, we first investigated its effect in the HepG2/ADR xenograft tumor mouse model. When the subcutaneous tumor grew to ~100 mm^3, the formulations were administered by tail vein injection. After 28 days of treatment, DOX and the LH/miR-375 showed limited antitumor effects in mice (Figure 7A and B). The LHD formulation showed a significantly greater antitumor effect than DOX or the LH/miR-375 did. Furthermore, the LHD/miR-375 showed a greater antitumor effect than the LHD did (Figure 7A and B). Importantly, no significant body weight loss was observed in the LHD- or LHD/miR-375-treated mice. In contrast, considerable weight loss was observed in the mice that were treated with free DOX (Figure 7C). In addition, the free DOX significantly elevated aspartate aminotransferase (AST) and alanine aminotransferase (ALT) levels. However, the LHD- and LHD/miR-375-treated mice showed lower AST and ALT levels than the mice treated with free DOX did, which indicate the low hepatic toxicity of the LHD and the LHD/miR-375 (Figure 7D). The low toxicity of the LHD formulation in

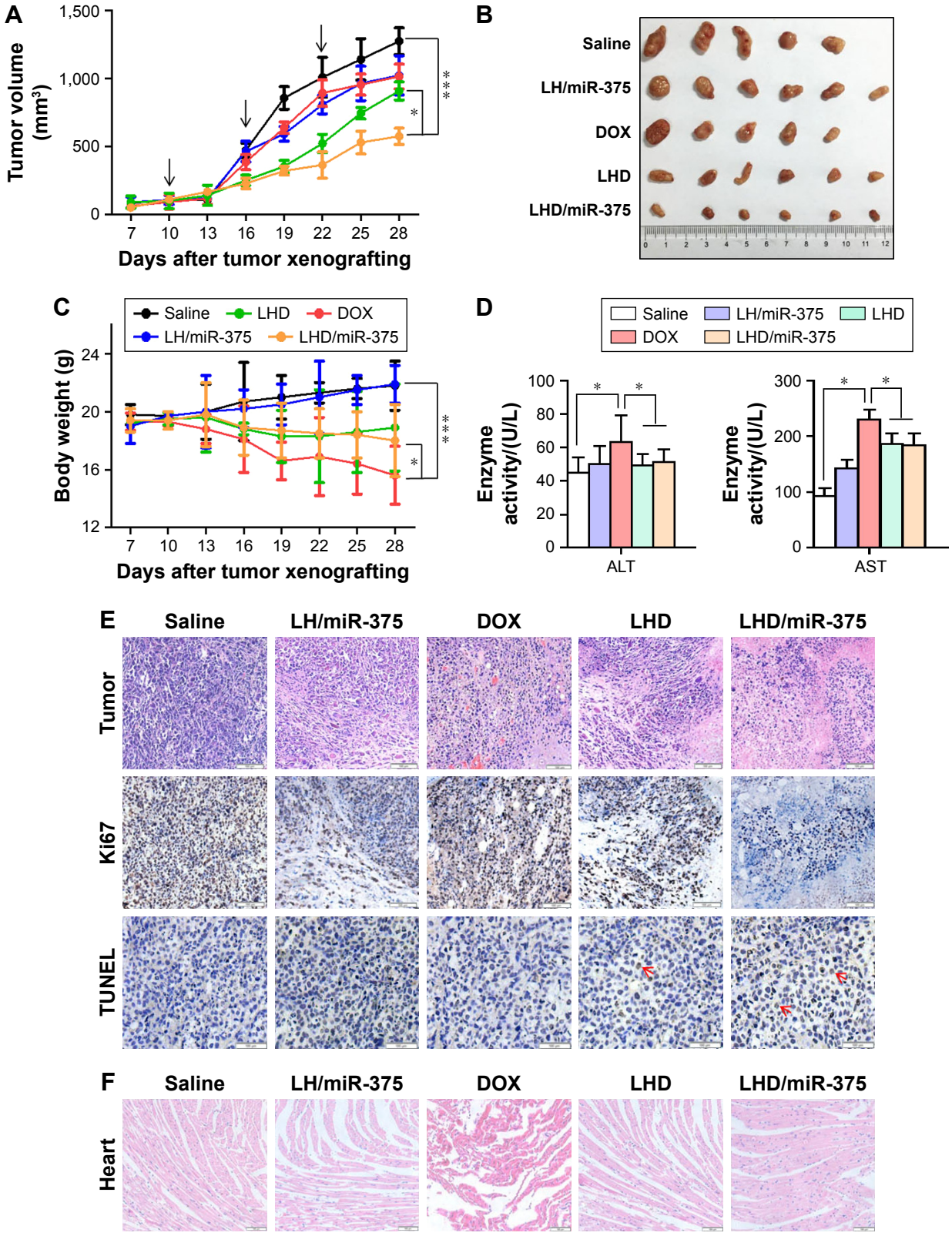

Figure 7 Antitumor effects of different formulations in BALB/c nude mice bearing HepG2/ADR tumors.

Notes: (**A**) Growth curves of tumors (n=6) treated with drugs. Arrows refer to the days of drug administrations. (**B**) Morphology of tumors excised from mice at the end of experiment. (**C**) Body weight changes of mice (n=6) during experimental period. (**D**) AST and ALT levels in the mice at the end of experiment. The serum (n=5 or 6) was collected after killing the mice, and AST and ALT levels were determined using an automatic biochemical analyzer. (**E**) Hematoxylin and eosin staining and immunohistochemistry analysis of tumor tissues. Arrows indicate the positive signal of TUNEL staining. (**F**) Evaluation of cardiac toxicity for DOX, LHD, LH/miR-375, and LHD/miR-375. *$P<0.05$; ***$P<0.001$. Magnification: 100× for tumor hematoxylin and eosin, Ki67 and heart Hematoxylin and eosin staining; 200× for TUNEL staining.

Abbreviations: ALT, alanine aminotransferase; AST, aspartate aminotransferase; DOX, doxorubicin hydrochloride; LH, lipid-coated hollow mesoporous silica nanoparticles; LHD, lipid-coated hollow mesoporous silica nanoparticles containing doxorubicin hydrochloride; TUNEL, terminal deoxynucleotidyl transferase dUTP nick end labeling.

mice is possibly due to its acid lability, which caused a low release of DOX in normal tissues, but a high release in tumor tissues although it was highly accumulated in both tissues. Moreover, the LHD/miR-375 were less toxic than the LHD, which indicates the excellent safety and advantage of using miR-375 to overcome MDR. Altogether, the results indicate that LHD/miR-375 enhance the therapeutic effect of DOX greatly and reduce the toxicity of DOX to mice.

We also examined the histological properties of the mouse tumor tissues and found that the LHD/miR-375 significantly inhibited tumor cell proliferation more than the LH/miR-375 or LHD did (Figure 7E). In addition, it was observed that the rate of apoptosis in the tumor tissues in LHD/miR-375-treated mice was high. Furthermore, the tumor cells treated with the LHD/miR-375 showed evident pyknosis and karyorrhexis. Necrosis was also observed in the tissues of LHD/miR-375-treated mice. In addition, hyperemia and myocardial fiber breakage were observed in the hearts of mice that were treated with free DOX; however, this was not observed in the LHD- or LHD/miR-375-treated mice (Figure 7F). These results indicate that the LHD/miR-375 inhibited tumor cell proliferation and reduced the cardiac toxicity of DOX.

As we observed a high accumulation of the LHD in the mouse livers, we explored the therapeutic potential of the LHD/miR-375 in primary HCC tumors. To mimic HCC pathology in human patients, a mouse model of Akt/Ras-induced primary HCC was developed by administering a hydrodynamic injection of plasmids carrying the two genes into mice, as previously described.[33] In hepatocytes, Akt promotes lipogenesis, whereas Ras promotes mitosis. Therefore, the synergistic effects of these two genes lead to tumor formation in the liver (Figure 8A). Three weeks after the Akt/Ras injection was administered, tumors were formed in the mice. This was followed by drug injection to the mice via the tail vein. After 7 drug doses were administered, it was observed that the average weight of the livers from LHD/miR-375-treated mice (5.1 g) was much smaller than that of the mice that were treated with free DOX (6.7 g), LH/miR-375 (8.5 g), or LHD (6.2 g) (Figure 8B and C). Importantly, the livers of mice that did not receive any drug treatment were more inhomogeneous and paler with more nodular lesions than those of the LHD- or LHD/miR-375-treated mice (Figure 8B). Correspondingly, the liver tissues of the LHD/miR-375-treated mice showed more normal tissues than those of the LHD-, LH/miR-375-, or free-DOX-treated mice (Figure 8B). Moreover, Ki67 staining demonstrated that there was reduced tumor cell proliferation in the livers of mice treated with LHD or LHD/miR-375 (Figure 8B). Similar to that observed in the mice with xenograft tumors, the mice with HCC that were treated with DOX showed significant body weight loss during the experiment (Figure 8D). In contrast, the LHD- and LHD/miR-375-treated mice did not show significant reduction in body weight as the DOX-treated mice did (Figure 8D). In addition, severe myocardial fiber breakage was observed in the DOX-treated mice; however, no significant myocardial injury was found in the LHD- or LHD/miR-375-treated mice (Figure 8E). Moreover, no obvious injury was found in the kidneys, lungs, or spleens of the LHD- or LHD/miR-375-treated mice (Figure 8E).

Taken together, the results from the studies conducted in the xenograft and primary tumor mouse models clearly demonstrate the therapeutic effects of the LHD/miR-375 in vivo. The higher antitumor effect of the LHD in comparison with that of the LH/miR-375 or free DOX suggests that the LHD generate an anti-MDR effect and hence improve the antitumor effect of DOX. The superior activity of the LHD/miR-375 over that of the LHD suggests that miR-375 confers an antitumor activity to the formulation by either overcoming MDR or inducing apoptosis. Moreover, the side effects of the LHD and LHD/miR-375 decreased compared to those of free DOX, which indicates that lipid-coated HMSN are an effective and safe carrier for co-delivering drugs and miRNA.

Conclusion

In this paper, we prepared lipid-coated HMSN for co-delivery of DOX and miR-375. LHD/miR-375 could be taken up efficiently by HepG2/ADR cells by phagocytosis, and clathrin- and caveolae-mediated endocytosis and keep a highly retained in these cells. LHD/miR-375 could exert dual effects to overcome DOX resistance in HepG2/ADR cells by evading P-gp efflux with LHD and inhibiting P-gp expression via miR-375, respectively. In both xenograft and primary HCC tumors, LHD/miR-375 could significantly enhance the antitumor effects of DOX and block the tumor growth. Moreover, LHD/miR-375 showed excellent safety in mice compared with DOX. Our study, for the first time, proved that miR-375 can generate a synergistic anti-MDR effect with HMSN, and thus improve the effects of chemotherapeutic agents. Significantly, our study provided an alternative option to overcome MDR in HCC and a potential therapeutic regimen for HCC treatment.

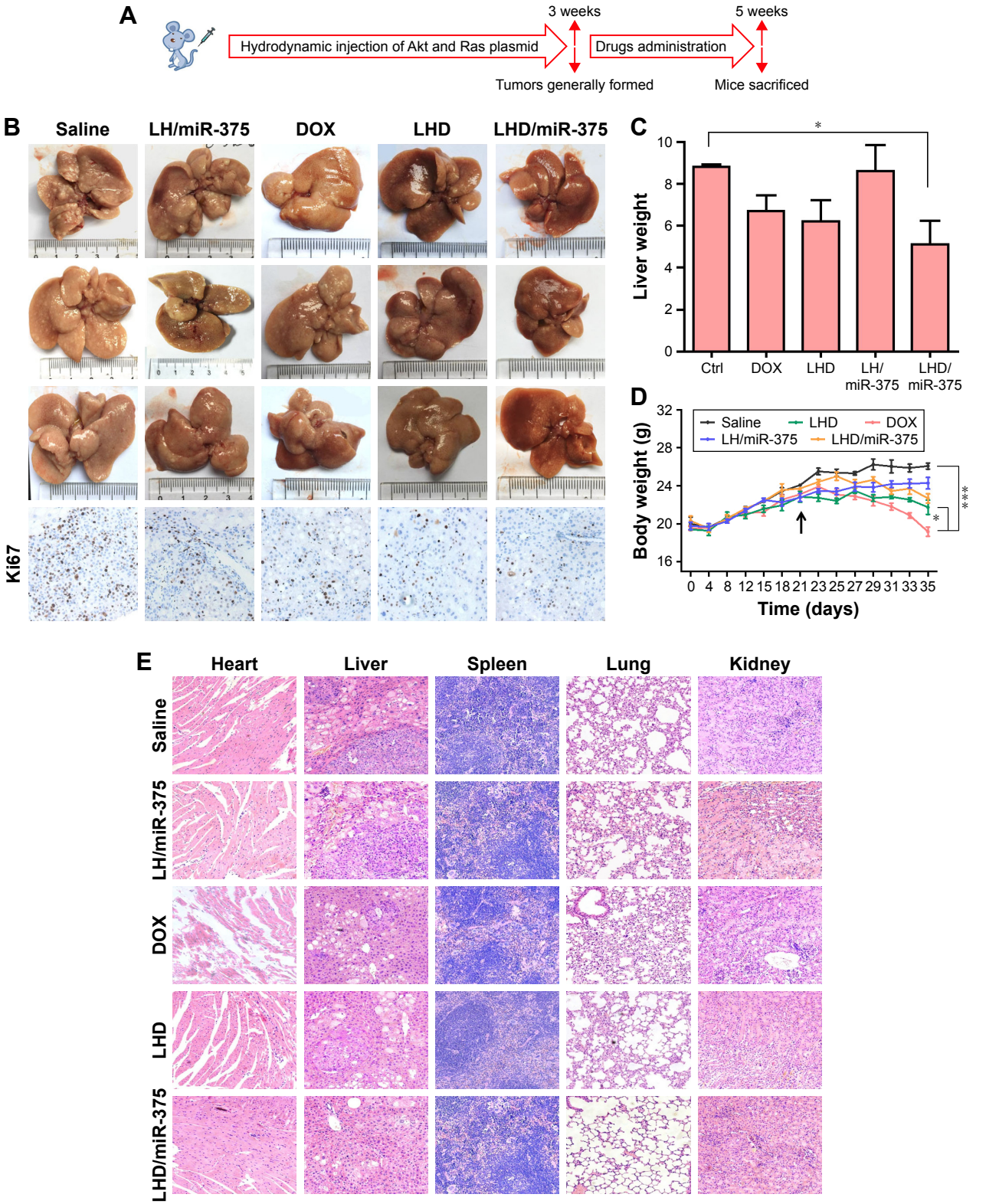

Figure 8 Antitumor effects of LHD/miR-375 in Akt/Ras-induced HCC mice.

Notes: (**A**) Overall diagram of study design. (**B**) Liver morphology and Ki67 analysis of mice treated with saline, free DOX, LH/miR-375, LHD, or LHD/miR-375 (equivalent of 6 mg/kg DOX or 4 nmol/kg miR-375) for 2 weeks. (**C**) The average liver weights for each group (n=3). (**D**) Body weight changes (n=3) during experimental period since the Akt/Ras injections. The arrow refers to the first time of drug administration. (**E**) Hematoxylin and eosin staining of HCC mouse organs after treatment with drugs. Mouse organs or tumor tissues were collected after killing the mice at the end of experiment. Magnification: 200×. *$P<0.05$; ***$P<0.001$.

Abbreviations: DOX, doxorubicin hydrochloride; HCC, hepatocellular carcinoma; LH, lipid-coated hollow mesoporous silica nanoparticles; LHD, lipid-coated hollow mesoporous silica nanoparticles containing doxorubicin hydrochloride.

Acknowledgments

This study was supported by National Foundation of Science of China (81370058, 81572723, 81402435), Innovation Foundation of Higher Education of China (2016JCTD109), and Graduates' Innovation Fund of Huazhong University of Science and Technology (No 0118650030).

Disclosure

The authors report no conflicts of interest in this work.

References

1. Jemal A, Bray F, Center MM, Ferlay J, Ward E, Forman D. Global cancer statistics. *CA Cancer J Clin*. 2011;61(2):69–90.
2. Pelgrift RY, Friedman AJ. Nanotechnology as a therapeutic tool to combat microbial resistance. *Adv Drug Deliv Rev*. 2013;65(13–14):1803–1815.
3. Sen R, Natarajan K, Bhullar J, et al. The novel BCR-ABL and FLT3 inhibitor ponatinib is a potent inhibitor of the MDR-associated ATP-binding cassette transporter ABCG2. *Mol Cancer Ther*. 2012;11(9):2033–2044.
4. Walsh N, Larkin A, Kennedy S, et al. Expression of multidrug resistance markers ABCB1 (MDR-1/P-gp) and ABCC1 (MRP-1) in renal cell carcinoma. *BMC Urol*. 2009;9(1):6.
5. Chen M, Xue X, Wang F, et al. Expression and promoter methylation analysis of ATP-binding cassette genes in pancreatic cancer. *Oncol Rep*. 2012;27(1):265–269.
6. Wersinger C, Rebel G, Lelong-Rebel IH. Detailed study of the different taurine uptake systems of colon LoVo MDR and non-MDR cell lines. *Amino Acids*. 2000;19(3–4):667–685.
7. Wei T, Chen C, Liu J, et al. Anticancer drug nanomicelles formed by self-assembling amphiphilic dendrimer to combat cancer drug resistance. *Proc Natl Acad Sci U S A*. 2015;112(10):2978–2983.
8. Huesker M, Folmer Y, Schneider M, Fulda C, Blum HE, Hafkemeyer P. Reversal of drug resistance of hepatocellular carcinoma cells by adenoviral delivery of anti-MDR1 ribozymes. *Hepatology*. 2002;36(4 Pt 1):874–884.
9. Barraud L, Merle P, Soma E, et al. Increase of doxorubicin sensitivity by doxorubicin-loading into nanoparticles for hepatocellular carcinoma cells in vitro and in vivo. *J Hepatol*. 2005;42(5):736–743.
10. Kovalchuk O, Filkowski J, Meservy J, et al. Involvement of microRNA-451 in resistance of the MCF-7 breast cancer cells to chemotherapeutic drug doxorubicin. *Mol Cancer Ther*. 2008;7(7):2152–2159.
11. Markman JL, Rekechenetskiy A, Holler E, Ljubimova JY. Nanomedicine therapeutic approaches to overcome cancer drug resistance. *Adv Drug Deliv Rev*. 2013;65(13–14):1866–1879.
12. Pan L, Liu J, He Q, Wang L, Shi J. Overcoming multidrug resistance of cancer cells by direct intranuclear drug delivery using TAT-conjugated mesoporous silica nanoparticles. *Biomaterials*. 2013;34(11):2719–2730.
13. Han M, Lv Q, Tang XJ, et al. Overcoming drug resistance of MCF-7/ADR cells by altering intracellular distribution of doxorubicin via MVP knockdown with a novel siRNA polyamidoamine-hyaluronic acid complex. *J Control Release*. 2012;163(2):136–144.
14. Susa M, Iyer AK, Ryu K, et al. Inhibition of ABCB1 (MDR1) expression by an siRNA nanoparticulate delivery system to overcome drug resistance in osteosarcoma. *PLoS One*. 2010;5(5):e10764.
15. Wang Y, Lieberman R, Pan J, et al. miR-375 induces docetaxel resistance in prostate cancer by targeting SEC23A and YAP1. *Mol Cancer*. 2016;15(1):70.
16. Wang C, Yang Q. Astrocyte elevated gene-1 and breast cancer (Review). *Oncol Lett*. 2011;2(3):399–405.
17. Lee SG, Jeon HY, Su ZZ, et al. Astrocyte elevated gene-1 contributes to the pathogenesis of neuroblastoma. *Oncogene*. 2009;28(26):2476–2484.
18. He XX, Chang Y, Meng FY, et al. MicroRNA-375 targets AEG-1 in hepatocellular carcinoma and suppresses liver cancer cell growth in vitro and in vivo. *Oncogene*. 2012;31(28):3357–3369.
19. Yoo BK, Chen D, Su ZZ, et al. Molecular mechanism of chemoresistance by astrocyte elevated gene-1. *Cancer Res*. 2010;70(8):3249–3258.
20. Emdad L, Das SK, Dasgupta S, Hu B, Sarkar D, Fisher PB. AEG-1/MTDH/LYRIC: signaling pathways, downstream genes, interacting proteins, and regulation of tumor angiogenesis. *Adv Cancer Res*. 2013;120:75–111.
21. Yoo BK, Emdad L, Lee SG, et al. Astrocyte elevated gene-1 (AEG-1): A multifunctional regulator of normal and abnormal physiology. *Pharmacol Ther*. 2011;130(1):1–8.
22. Yang T, Zhao P, Rong Z, et al. Anti-tumor efficiency of lipid-coated cisplatin nanoparticles co-loaded with microRNA-375. *Theranostics*. 2016;6(1):142–154.
23. Li N, Huang C, Luan Y, Song A, Song Y, Garg S. Active targeting co-delivery system based on pH-sensitive methoxy-poly(ethylene glycol)2K-poly(epsilon-caprolactone)4K-poly(glutamic acid)1K for enhanced cancer therapy. *J Colloid Interface Sci*. 2016;472:90–98.
24. Chen F, Hong H, Zhang Y, et al. In vivo tumor targeting and image-guided drug delivery with antibody-conjugated, radiolabeled mesoporous silica nanoparticles. *ACS Nano*. 2013;7(10):9027–9039.
25. Asefa T, Tao Z. Biocompatibility of Mesoporous Silica Nanoparticles. *Chem Res Toxicol*. 2012;25(11):2265–2284.
26. Fang X, Zhao X, Fang W, Chen C, Zheng N. Self-templating synthesis of hollow mesoporous silica and their applications in catalysis and drug delivery. *Nanoscale*. 2013;5(6):2205–2218.
27. Guo S, Wang Y, Miao L, et al. Lipid-coated cisplatin nanoparticles induce neighboring effect and exhibit enhanced anticancer efficacy. *ACS Nano*. 2013;7(11):9896–9904.
28. Tang F, Li L, Chen D. Mesoporous silica nanoparticles: synthesis, biocompatibility and drug delivery. *Adv Mater*. 2012;24(12):1504–1534.
29. Chakravarty R, Goel S, Hong H, et al. Hollow mesoporous silica nanoparticles for tumor vasculature targeting and PET image-guided drug delivery. *Nanomedicine (Lond)*. 2015;10(8):1233–1246.
30. Chen F, Hong H, Shi S, et al. Engineering of hollow mesoporous silica nanoparticles for remarkably enhanced tumor active targeting efficacy. *Sci Rep*. 2014;4:5080.
31. Liu J, Stace-Naughton A, Brinker CJ. Silica nanoparticle supported lipid bilayers for gene delivery. *Chem Commun (Camb)*. 2009;(34):5100–5102.
32. Gao Y, Chen Y, Ji X, et al. Controlled intracellular release of doxorubicin in multidrug-resistant cancer cells by tuning the shell-pore sizes of mesoporous silica nanoparticles. *ACS Nano*. 2011;5(12):9788–9798.
33. Ho C, Wang C, Mattu S, et al. AKT (v-akt murine thymoma viral oncogene homolog 1) and N-Ras (neuroblastoma ras viral oncogene homolog) coactivation in the mouse liver promotes rapid carcinogenesis by way of mTOR (mammalian target of rapamycin complex 1), FOXM1 (forkhead box M1)/SKP2, and c-Myc pathways. *Hepatology*. 2012;55(3):833–845.
34. Chen X, Calvisi DF. Hydrodynamic transfection for generation of novel mouse models for liver cancer research. *Am J Pathol*. 2014;184(4):912–923.
35. Bao Y, Yin M, Hu X, et al. A safe, simple and efficient doxorubicin prodrug hybrid micelle for overcoming tumor multidrug resistance and targeting delivery. *J Control Release*. 2016;235:182–194.